International Immunopharmacology 152 (2025) 114406

Contents lists available at ScienceDirect

International Immunopharmacology

journal homepage: www.elsevier.com/locate/intimp

Luteolin attenuates cadmium neurotoxicity by suppressing glial inflammation and supporting neuronal survival

Hui-Yong Ma [a,1], Jing Wang [a,1], Jun Wang [a], Zhe Guo [b], Xiao-Yan Qin [a], Rongfeng Lan [b,*], Yang Hu [a,*]

[a] Key Laboratory of Ecology and Environment in Minority Areas National Ethnic Affairs Commission, Center on Translational Neuroscience, College of Life and Environmental Sciences, Minzu University of China, Beijing 100081, China.
[b] Department of Cell Biology & Medical Genetics, School of Basic Medical Sciences, Shenzhen University Medical School, Shenzhen 518060, China

ARTICLE INFO

Editor name: Yi-Chao Zheng

Keywords:
Astrocyte
BDNF
Cadmium
Luteolin
Microglia

ABSTRACT

Cadmium (Cd), a neurotoxic metal, is associated with the development of neurological disorders. This study investigated the neuroprotective effects of Luteolin against Cd-induced toxicity in cultured cells and mouse models. Our findings demonstrate that Luteolin protects hippocampal neurons from Cd toxicity and mitigates Cd-triggered inflammatory responses in microglial BV2 cells. In Cd-exposed mice, symptoms such as weight loss, motor retardation, multi-organ damage, and cognitive deficits were observed. Remarkably, Luteolin treatment reversed these effects, repaired organ damage, and restored learning and memory abilities. Mechanistically, Cd toxicity induced significant upregulation of pro-inflammatory factors and neuroinflammation in the hippocampus and prefrontal cortex, including elevated glial cell markers (IBA1, GFAP, and CD68) and reduced neuronal marker MAP2. Luteolin counteracted these adverse effects by inhibiting the Notch1/Hes1 inflammatory signaling axis and restoring the BDNF-TrkB/AKT1 signaling axis, thereby promoting neuronal survival. These results highlight the potential of Luteolin as a natural neuroprotective agent against Cd-induced neurotoxicity, offering a promising therapeutic strategy for mitigating Cd-related neurological damage.

1. Introduction

Cd ranks seventh among the 275 new toxic substances identified by the Agency for Toxic Substances and Disease Registry in 2022, highlighting its significance as a major environmental pollutant [1]. Cd accumulates in the human body through industrial and domestic pollution and can cross the blood-brain barrier (BBB), leading to systemic dysfunction, including damage to the central nervous system (CNS) [2,3]. As a critical environmental risk factor, Cd exposure has been linked to various neurological disorders, such as depression, Alzheimer's disease (AD), Parkinson's disease (PD), and schizophrenia [4–8]. The neurotoxicity of Cd manifests through its ability to disrupt mitochondrial activity, impair synaptic function, and alter neurotransmitter release, calcium homeostasis, and cognitive processes [9]. Although previous studies have implicated inflammation, oxidative stress, and neuronal apoptosis in Cd-induced neurotoxicity, the precise mechanisms remain poorly understood [10–12]. Especially, the role of Cd in the progression of neurodegenerative diseases is not fully elucidated. Additionally, there is a lack of research on natural products capable of mitigating Cd toxicity, and no effective treatments currently exist for metal-induced neurotoxicity or related neurological disorders. Therefore, further investigation is needed to evaluate Cd-induced neuronal

Abbreviations: AKT1, AKT serine/threonine kinase 1; ANOVA, Analysis of Variance; BDNF, Brain Derived Neurotrophic Factor; CA1, Cornu Ammonis 1; CAT, Catalase; Cd, Cadmium; CD68, Macrophage Antigen CD68/Macrosialin; C/EBP beta, CCAAT/enhancer binding protein beta; CNS, Central Nervous System; DAPI, 4′,6-diamidino-2-phenylindole; DG, Dentate Gyrus; ELISA, Enzyme-Linked Immunosorbent Assay; FST, Forced Swimming Test; GFAP, Glial Fibrillary Acidic Protein; HIP, Hippocampus; IBA1, Ionized Calcium-Binding Adapter Molecule 1/Allograft Inflammatory Factor 1; IL-1B, Interleukin-1 beta; IL-10, Interleukin 10; IL-6, Interleukin 6; LDH, Lactate dehydrogenase; MAP2, Microtubule Associated Protein 2; MDA, Malondialdehyde; MWM, Morris Water Maze; Nos2, Nitric Oxide Synthase 2; TrkB, Neurotrophic receptor tyrosine kinase 2; OFT, Open Field Test; PFC, Prefrontal Cortex; RBPJ, Recombination Signal Binding Protein for Immunoglobulin kappa J Region; SOD, Superoxide Dismutase; T-AOC, Total Antioxidant Capacity; TNF, Tumor Necrosis Factor..

* Corresponding authors.
E-mail addresses: lan@szu.edu.cn (R. Lan), yang.hu@muc.edu.cn (Y. Hu).
[1] These authors contributed equally: H-Y Ma and J. Wang.

https://doi.org/10.1016/j.intimp.2025.114406
Received 9 December 2024; Received in revised form 19 February 2025; Accepted 1 March 2025
Available online 10 March 2025
1567-5769/© 2025 Elsevier B.V. All rights are reserved, including those for text and data mining, AI training, and similar technologies.

Table 1
Primers used RT-PCR.

Gene ID	Gene symbol	Sense (5′–3′)	Anti-sense (5′–3′)
21,926	*Tnf*	CTATGGCCCAGACCCTCACA	TCTTGACGGCAGAGAGGAGG
16,193	*Il6*	GCTACCAAACTGGATATAATCAGGA	CCAGGTAGCTATGGTACTCCAGAA
16,176	*Il1b*	GAAATGCCACCTTTTGACAGTG	TGGATGCTCTCATCAGGACAG
18,126	*Nos2*	GAATCTTGGAGCGAGTTGTGGA	GTGAGGGCTTGGCTGAGTGAG
16,153	*Il10*	GCTCTTACTGACTGGCATGAG	CGCAGCTCTAGGAGCATGTG
11,461	*Actb*	GGCTGTATTCCCCTCCATCG	CCAGTTGGTAACAATGCCATGT

toxicity and its underlying mechanisms.

Natural active compounds represent a promising avenue for developing therapies against neurodegenerative diseases [13,14]. In our previous studies, we found that natural product molecules such as Paeoniflorin and Salidroside, exhibit significant anti-Cd neurotoxicity effects and can reverse Cd-induced learning and memory deficits in experimental mice [15,16]. Luteolin, a naturally occurring tetrahydroxy-flavone found in broccoli, carrots, and cauliflower, possesses diverse pharmacological properties, including antiviral, antioxidant, and anti-inflammatory activities [17–21]. Recent studies demonstrated that Luteolin protects SH-SY5Y cells from zinc-induced apoptosis, regulates redox imbalance, and inhibits copper-induced apoptosis mediated by the Caspase family [22–24]. Moreover, Luteolin, with its 5,7-dihydroxychroman-4-one backbone, enhances StAR expression, thereby promoting testosterone production in testicular Leydig cells [25]. It also ameliorates cognitive deficits and mitigates Aβ-induced oxidative stress, mitochondrial dysfunction, and neuronal apoptosis in 3xTg-AD mice [26]. These findings suggest Luteolin may exert neuroprotective effects and counteract Cd-induced toxicity.

In this study, we employed a mouse model of Cd toxicity and an in vitro cellular model, as previously described [16,27,28]. We investigated the neuroprotective effects of Luteolin on Cd-exposed cultured cells and mice, focusing on its ability to attenuate Cd toxicity, enhance cell survival, and ameliorate behavioral abnormalities and pathological changes in mice. Additionally, we explored the underlying molecular mechanisms of Luteolin's protective actions.

2. Materials and method

2.1. Cells and chemicals

Rat hippocampal neurons were prepared as previously described [29,30]. Luteolin (#SM2045, Beyotime Biotechnology) was dissolved in dimethyl sulfoxide (DMSO) to prepare a 20 mM stock solution. LY294002 (#S1737-5 mg, Beyotime Bio-Tech Co., Ltd., Shanghai), a PI3K inhibitor, was used at a concentration of 10 μM. *Z*-DEVD-FMK (#IZ0030, Solarbio Science & Technology Co., Ltd., Beijing), a Caspase-3 inhibitor, was used at 0.4 μM. Mouse microglia BV2 cells were cultured in DMEM medium supplemented with 10 % fetal bovine serum (FBS), 100 U/mL penicillin, and 100 μg/mL streptomycin at 37 °C in a 5 % CO_2 atmosphere, as previously described [31], mouse microglia BV2 cells were cultured in DMEM medium containing 10 % FBS, penicillin 100 U/mL, and streptomycin 100 μg/mL at 37 °C and 5 % CO_2. Cells were passaged every 2–3 days, and log-phase cells were used for experiments.

2.2. Immunofluorescence imaging in cultured cells

Immunofluorescence imaging was performed as previously established [15]. Neurons or BV2 cells were fixed with 4 % paraformaldehyde for 15 min, permeabilized with 0.2 % Triton X-100 for 10 min, and blocked with 10 % FBS in PBS to prevent non-specific binding. Cells were then incubated with primary antibodies against MAP2 (#17490–1-AP, Proteintech) or IBA1 (#019–19,741, Wako), followed by Alexa Fluor 594-conjugated secondary antibodies. Nuclei were counterstained with DAPI (#D9542, Sigma-Aldrich), and images were acquired using a Leica TCS SP8 confocal microscope.

2.3. Cell viability assay and ATP measurements

Cell Viability Assay: Cells seeded in 96-well plates were treated with the indicated drugs, followed by incubation with 10 μL of WST-1 solution (#C0035, Beyotime Biotechnology) for 2 h. Absorbance was measured at 450 nm, and results were normalized to the control group.

ATP Measurements: Cells were lysed with lysis buffer (#BC0305, SolarBio Life Sciences; 1 mL per 5×10^6 cells) and centrifuged at 10,000 $\times g$ for 10 min at 4 °C. The supernatant was collected, mixed with 500 μL of chloroform, and vortexed thoroughly. After centrifugation at 10,000 $\times g$ for 3 min at 4 °C, the supernatant was collected and kept on ice for ATP measurement. Absorbance was measured at 340 nm, and relative ATP levels were normalized to the control group.

2.4. Western blotting of cellular samples

After treatment, proteins were extracted from hippocampal neurons and quantified using a BCA kit (#PC0020, Solarbio Life Sciences). Equal amounts of proteins were separated by 10 % SDS-PAGE and transferred to nitrocellulose membranes. Membranes were blocked with 5 % skimmed milk for 1 h, washed three times with TBST, and incubated overnight at 4 °C with the following primary antibodies: (BDNF, #ab108319, abcam; AKT1, #AF0045, Beyotime Biotechnology; Phospho-AKT1 (Ser473), #AF1546, Beyotime Biotechnology; Cleaved-Caspase 3, #9664, Cell Signaling Technology; Bcl2, #bs-0032R, Bioss; Beta-actin, #AF0003, Beyotime Biotechnology). After incubation with secondary antibodies, protein bands were visualized using a chemiluminescence imaging system (Odyssey CLX). Band intensities were quantified using optical density analysis and normalized to Beta-actin.

2.5. RT-PCR of genes in BV2 cells

Total RNA was extracted using Trizol reagent (#15596026, Invitrogen) and 1.0 μg of RNA was reverse transcribed in to cDNA using the EasyQuick RT MasterMix Kit (#CW 2019 M, Cowin Bio.) The cDNA was diluted 1:10 with DEPC-treated water. Quantitative PCR was performed in a 10 μL reaction using the Light Cycler 96 Real-Time PCR System (Roche) with 2× RealStar Green Fast Mixture (#A301–05, GenStar) and primers listed in Table 1. Each template was run in triplicate, and five biological replicates were analyzed. Relative gene expression changes were calculated using the 2^(-ΔΔCt) method.

2.6. Animal

C57BL/6 J male mice (8 weeks old, $n = 40$) were obtained from Charles River Laboratories (Beijing). The animals were randomly divided into four groups ($n = 10$ per group): Control, $CdCl_2$ (2 mg/kg body weight), $CdCl_2$ (2 mg/kg) + Luteolin (50 mg/kg), and Luteolin (50 mg/kg) [32,33]. $CdCl_2$ was administered via intraperitoneal injection every two days for 42 days, while the control group received saline. Luteolin was dissolved in dimethyl sulfoxide (DMSO) to prepare a 100 mg/mL stock solution, which was then diluted in saline to a final concentration of 5 mg/mL. The solution was administered by oral gavage at

~0.2 mL per mouse, adjusted for body weight. All animal procedures were conducted in accordance with the National Institutes of Health Laboratory Animal Care and Use Guidelines (NIH Publication No. 80–23) and approved by the Ethics Committee of Animal Care and Use at Minzu University of China (ECMUC2021006AA).

2.7. Behavioral experiments

Morris water maze (MWM) test: The MWN test was performed to evaluate cognitive ability as previously described [34,35]. The test consisted of two phases over 7 days. (1) Acquisition training (Days 1–6): Mice were trained to locate a hidden platform (10 cm in diameter) submerged 1 cm below the water surface in a circular pool (110 cm in diameter, 50 cm in height). Each mouse was allowed 60 s to find the platform. If unsuccessful, the mouse was guided to the platform and allowed to remain there for 15 s to reinforce spatial memory. (2) Probe test (Day 7): The platform was removed, and mice were allowed to swim freely for 60 s. The time spent in the target quadrant, distance traveled, and latency to cross the former platform location were recorded using a video tracking system (Taimeng WMT-100).

The Y-Maze test was used to assess exploratory behavior and spatial memory [36]. The maze consisted of three arms (30 cm × 6 cm × 15 cm) arranged at 120° angles. Mice were placed at the end of one arm and allowed to explore freely for 10 min. An entry was recorded when all four limbs entered an arm. A correct alternation was defined as entering a new arm different from the previous two. The total number of arm entries and spontaneous alternations were calculated.

The forced swim test (FST) was conducted to evaluate depression-like behavior [37]. Mice were placed in a cylindrical tank (10 cm in diameter, 38 cm in height) filled with water (25 ± 1 °C, 25 cm deep) and allowed to swim for 6 min. The first minute was excluded for acclimatization, and immobility time during the remaining 5 min was recorded using Taimeng FST-100 software. The pole test was performed to assess motor coordination and bradykinesia as previously described [38].

The Wire-Hang test evaluated grip strength, endurance, and motor coordination [39]. Mice were placed on a horizontal wire, and the time until they fell was recorded. Scoring was based on hindlimb engagement: 3 points (both hindlimbs hooked), 2 points (one hindlimb hooked), or 1 point (no hindlimbs hooked). Hanging time was scored as follows: 0–4 s (0 points), 5–9 s (1 point), 10–14 s (2 points), 15–19 s (3 points), 20–24 s (4 points), 25–29 s (5 points), or ≥ 30 s (6 points).

The Open Field Test (OFT) was used to measure locomotor activity and anxiety-like behavior [40]. Mice were placed in a square arena (60 cm × 60 cm × 25 cm) with a central zone (30 cm × 30 cm) and allowed to explore for 10 min. The time spent and distances traveled in the central zone were recorded using video tracking software.

2.8. LDH activity assay

Lactate dehydrogenase (LDH) activity in mouse serum and hippocampal tissue was measured using a commercial kit (#BC5280, Solarbio Life Sciences). Serum was used directly, while tissues were homogenized in lysis buffer (0.1 g tissue per 1 mL buffer). Absorbance was measured at 450 nm, and LDH activity was calculated based on a standard curve.

2.9. Assay of oxidative stress and inflammatory cytokines

Oxidative stress markers in the prefrontal cortex were measured using the following kits as described [31]. Superoxide dismutase (SOD) assay kit (#A001–3-2), Catalase (CAT) assay kit (#A007–1-1), and Malondialdehyde (MDA) assay Kit (#A003–1-2) were from Nanjing Jiancheng Bioengineering Institute.

Inflammatory cytokines (TNF, IL-1B, IL-6, and IL-10) in the prefrontal cortex were quantified using ELISA kits (#H052–1-1, #H002–1-2, #H007–1-1, and #H009–1-2, respectively, Nanjing Jiancheng Bioengineering Institute.

2.10. RT-PCR of genes in brain tissues

Total RNA was extracted from hippocampal tissue using Trizol reagent (#15596026, Invitrogen) and reverse-transcribed into cDNA as described in Section 2.5 [15]. Quantitative PCR was performed using primers listed in Table 1.

2.11. Hematoxylin-eosin (H&E) staining

Animal handling and tissue section staining were performed as previously described [15]. Briefly, mice were anesthetized with isoflurane, and blood samples were collected from the ocular vein to isolate serum. The thoracic and abdominal cavities were opened, and saline perfusion was performed through the left ventricle to remove residual blood. Tissues were then harvested. For immunofluorescence (IF) and immunohistochemistry (IHC), tissues were immediately immersed in 4 % paraformaldehyde and fixed for 24 h. For RT-PCR and Western blotting analysis, tissues were snap-frozen and stored at −80 °C. Tissue sections of the liver, kidney, and testis were stained using an H&E staining kit (#G1003, Servicebio) following the manufacturer's protocol.

2.12. Immunofluorescence imaging in brain tissues

Prefrontal cortex (PFC) and hippocampus (HIP) sections were fixed, dehydrated, and blocked with 5 % goat serum (#SL038, Solarbio) and 0.4 % Triton X-100. Sections were incubated overnight at 4 °C with primary antibodies (MAP2, #17490–1-AP, Proteintech; GFAP, #16825–1-AP, Proteintech; IBA1, #019–19,741, Wako; CD68, #ab53444, Abcam), followed by secondary antibodies. Images were acquired using a Leica TCS SP8 confocal microscope. Fluorescence intensity, microglia branch length, and branching points were analyzed using Image J software.

2.13. Immunohistochemistry (IHC)

IHC was performed on PFC and HIP sections as previously described [41]. Antibodies included MAP2 (#17490–1-AP, Proteintech), GFAP (#16825–1-AP, Proteintech), TNF (#AF8208, Beyotime Biotechnology), and IBA1 (1:100, #019–19,741). Positive cells were quantified using Image Pro Plus 6.0 software (Media Cybernetics, Inc.)

2.14. Western blotting of tissue samples

Hippocampal proteins were extracted, quantified using a BCA kit (#PC0020, Solarbio Life Sciences), and subjected to Western blotting as described in Section 2.4 [15]. Primary antibodies included MAP2 (#17490–1-AP), IBA1 (#10904–1-AP), RBPJ (#14613–1-AP), and GFAP (#16825–1-AP) were from Proteintech; TrkB (#4603) from Cell Signaling Technology; Phospho-TrkB (Tyr817) (#AF1963), Notch1 (NTM) (#AF5249), Hes1 (#AF2167), and NF-κB p65 (#AF0246) from Beyotime Biotechnology; NF-κB p65 (phosphor Ser536) (#BD-PP0191) and COP1 (#BD-PP0477) from Biodragon; and C/EBP beta (#bs-1396R) from Bioss antibodies.

2.15. Statistical analysis

Data are expressed as Mean ± S.E.M. Differences between groups were analyzed using one-way or two-way ANOVA (for repeated measures) or the Kruskal-Wallis test for nonparametric data. Significance was set at $^{*}p < 0.05$.

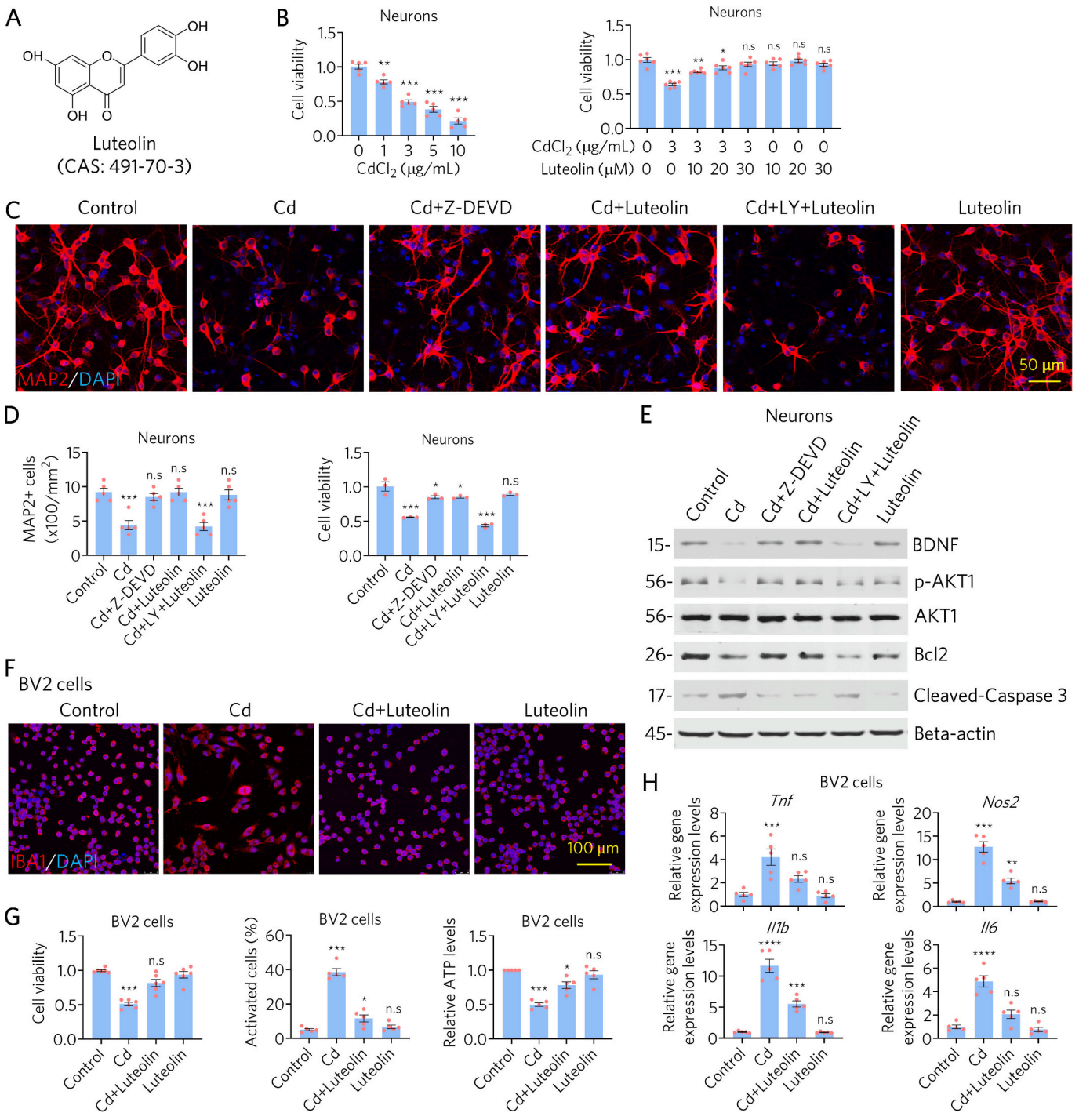

Fig. 1. Luteolin protects cultured neurons and glia cells from Cd-induced toxicity.

(A) Chemical structure of Luteolin. (B) In cultured hippocampal neurons, Cd exposure significantly reduced cell viability in a dose-dependent manner, an effect that was attenuated by Luteolin in a dose-dependent manner. Cell viability was assessed as described in the Materials and Methods section. (C) Luteolin (20 μM) preserved the integrity of hippocampal neurons against Cd-induced toxicity. Microscopic images were captured 24 h after treatment. Representative immunofluorescence images show co-staining with MAP2 (neuronal marker) and DAPI (nuclear stain). *Z*-DEVD, Z-DEVD-FMK (inhibitor of Caspase-3). LY, LY294002, an inhibitor of PI3K (10 μM). (D) Luteolin attenuated Cd-induced cell damage, similar to the effect of Z-DEVD-FMK, while LY294002 blocked Luteolin's protective effect. Cell counts were based on MAP2 staining, and cell viability was assayed. (E) Representative Western blotting images show protein levels of BDNF, p-AKT1, AKT1, Bcl2, Cleaved-Caspase 3 and Beta-actin in hippocampal neurons. (F) Luteolin inhibited Cd-induced cell death and activation of BV2 microglial cells. Representative immunofluorescence images show co-staining with IBA1 (microglial marker) and DAPI. (G) Cell viability was measured and the activated BV2 cells exhibited larger cell bodies and occasionally multiple nuclei. ATP levels were quantified using an ATP assay kit. (H) RT-PCR analysis revealed mRNA levels of inflammatory factors (*Tnf*, *Il1b*, *Il6* and *Nos2*) in BV2 cells. Statistical significance was determined by one-way ANOVA followed by Dunnett's multiple comparisons test. *, $p < 0.05$; **, $p < 0.01$; ***, $p < 0.001$; ****, $p < 0.0001$; n.s, not significant.

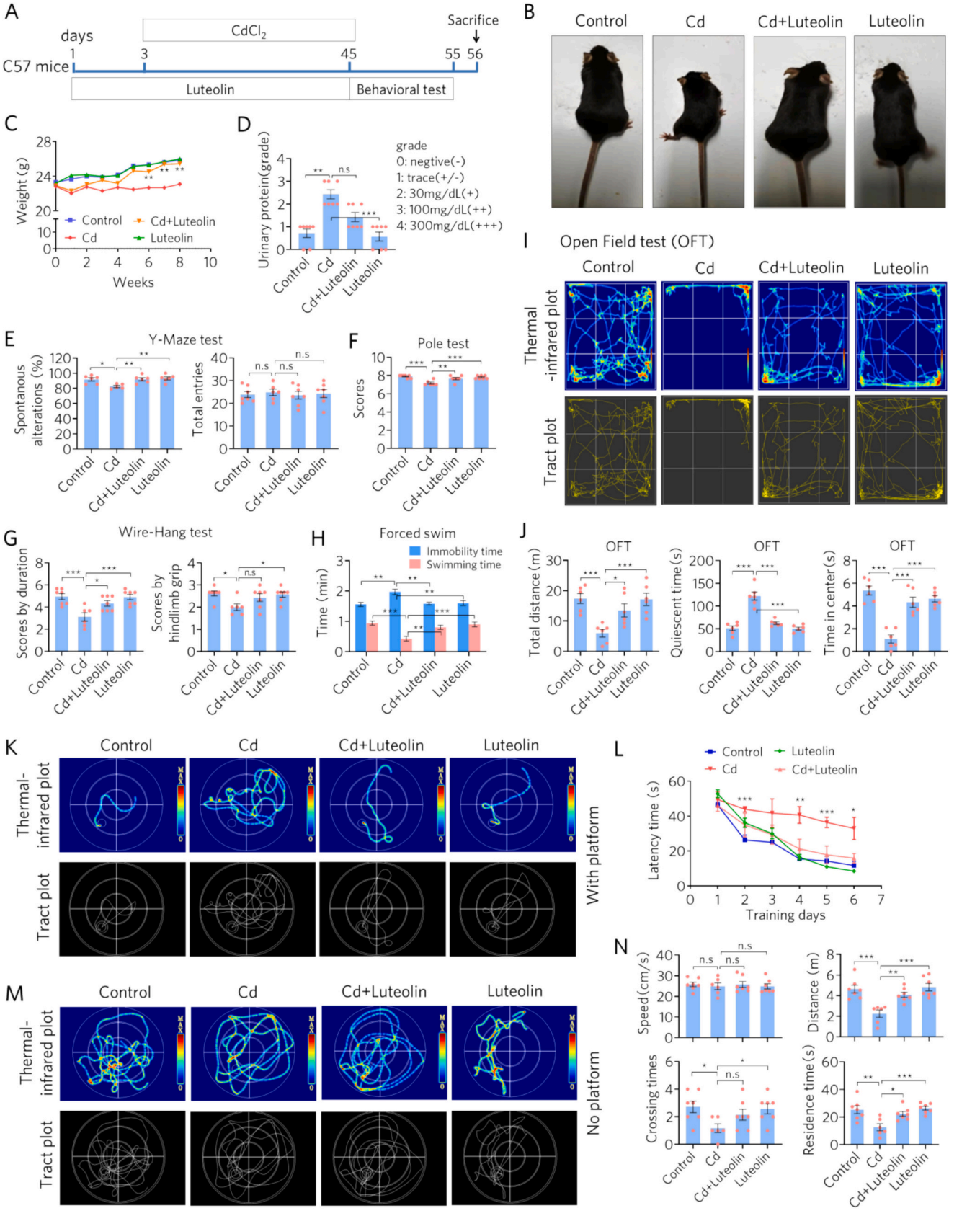

(caption on next page)

Fig. 2. Luteolin restored Cd-induced AD-like and depressive-like behaviors in mice.
(A) Timeline of animal experimental procedures. (B) Appearance of a wild-type mice (control group), Cd mice, Cd + Luteolin mice and Luteolin mice. (C) Body weight was measured every two weeks. Luteolin prevented Cd-induced weight loss. (D) Urinary protein was assessed with a mouse MAU (Micro albumin urea) kit. Luteolin reduced the Cd-induced increase in urinary protein. Kruskal-Wallis test; **, $p < 0.01$. (E) Spontaneous alternations and number of arm entries in the Y-maze test. Luteolin rescued the reduction in spontaneous alternations caused by Cd. (F) Pole climbing time (average turn time) in the pole test. Luteolin improved the motor performance of Cd-exposed mice ($p = 0.0036$). (G) Immobility time and active time in the forced swimming test. Cd-exposed mice exhibited prolonged immobility, indicating depressive-like behavior, which was ameliorated by Luteolin. (H) Number of grasps by fore and hind limbs in the tail suspension test. Luteolin improved the performance of Cd-exposed mice. (I) Representative movement trajectories in the open field test. Luteolin enhanced the exploratory behavior of Cd-exposed mice. (J) Total distance moved, freezing time, and distance moved in the central zone in the open field test. Luteolin restored the impaired performance of Cd-exposed mice. (K) Representative swim paths and thermal-infrared trajectories/occupancy plots on day 6 of the Morris water maze (MWM) acquisition phase. The target platform location is marked with a red circle. Luteolin improved the performance of Cd mice in the acquired training part of the MWM test. (L) Escape latency time of the acquired training (with platform) part of the MWM test were detected. Luteolin improved the learning speed of Cd mice in the acquired training part of the MWM test. (M) In the probe tracking portion of the MWM test, representative swim paths and thermal-infrared trajectories/occupancy or tract plots of mice were recorded as in (K) on behavioral day 7, the location of the underwater platform is marked with a red circle to represent the target area. Luteolin improved the performance of Cd mice in the probe trail part of the MWM test. (N) In the probe trial, the number of platform crossings, total distance traveled, swimming speed, and time spent in the target quadrant were measured. Luteolin improved the spatial memory of Cd-exposed mice. In this figure, statistical analysis was carried out in C, D, E, F, G, H, J and N by one-way ANOVA, post hoc Dunnett's multiple comparison test. Whereas in L, one-way RM ANOVA, post hoc Dunnett's test was performed. (For interpretation of the references to colour in this figure legend, the reader is referred to the web version of this article.)

3. Results

3.1. Luteolin protects hippocampal neurons and glia cells from cd-induced toxicity

The protective properties of Luteolin were first investigated in vitro by incubating cultured mouse hippocampal neurons with Cd at set concentrations for 24 h, either alone or in combination with Luteolin (Fig. 1A and B). Cd exposure (1–10 μg/mL) significantly and dose-dependently reduced hippocampal neuron viability after 24 h. At 3 μg/mL, Cd decreased cell viability to approximately 50 % ($p = 0.0015$), a concentration subsequently used for further experiments. Co-incubation with Luteolin (10–30 μM) dose-dependently attenuated Cd-induced toxicity and restored cell viability. Notably, Luteolin alone had no significant effect on cell viability.

Immunofluorescence staining of cultured neurons using an antibody specific for MAP2, a neuronal marker, revealed that Cd-induced toxicity impaired neuronal integrity and cell viability (Fig. 1C and D). In contrast, Luteolin preserved cell viability and maintained neuronal integrity. The protective effect of Luteolin was comparable to that of *Z*-DEVD-FMK (0.4 μM), a Caspase-3 inhibitor, suggesting that Cd-induced toxicity primarily triggers neuronal apoptosis. However, the protective effect of Luteolin was blocked by LY294002, a phosphatidylinositol 3 (PI3) kinase inhibitor (Fig. 1C and D), indicating that Luteolin's action depends on the BDNF-TrkB/AKT1 pathway, which inhibits apoptosis and promotes neuronal survival. To confirm this mechanism, we analyzed protein expression levels by Western blotting (Fig. 1E). Cd toxicity significantly downregulated BDNF, p-AKT1, and Bcl2 (an endogenous apoptosis inhibitor), while upregulating cleaved-Caspase 3, the active form of the apoptotic enzyme. Luteolin restored the expression levels of these proteins, similar to the effect of Caspase 3 inhibitors, and attenuated Cd-induced toxicity. This restoration was disrupted by PI3K inhibition, further supporting the role of the BDNF-TrkB/AKT1 signaling axis in Luteolin's protective effects.

Next, we examined the protective effects of Luteolin on the microglial cell line BV2. Immunofluorescence staining with an antibody against IBA1, a marker of microglial activation, showed that Cd toxicity significantly increased IBA1 expression in BV2 cells and induced morphological changes, including enlarged cell bodies and partial multinucleation (Fig. 1F and G). Luteolin restored IBA1 expression, inhibited morphological changes, and reduced cell viability and ATP levels, thereby suppressing BV2 cell activation. RT-PCR analysis revealed that Cd exposure (1.5 μg/mL) significantly increased the mRNA levels of inflammatory cytokines, including *Tnf* ($p = 0.0001$), *Nos2* ($p < 0.0001$), *Il1b* ($p < 0.0001$), and *Il6* ($p < 0.0001$), compared to the control group. Luteolin effectively inhibited the upregulation of these inflammatory factors (Fig. 1H). In summary, Luteolin protects hippocampal neurons and glial cells from Cd-induced toxicity by restoring the BDNF-TrkB/AKT1 signaling axis, inhibiting apoptosis, and suppressing neuroinflammation.

3.2. Luteolin restored cd-induced cognitive deficits and depressive-like behaviors in mice

Given Luteolin's protective effects against Cd-induced toxicity in vitro, we next evaluated its behavioral effects in vivo. A chronic Cd-exposed C57BL/6 J mouse model was established by administering 2 mg/kg $CdCl_2$ every other day for 6 weeks. Treatment groups included Cd + Luteolin and Luteolin alone (Fig. 2A). Before sacrifice, photographs revealed that Cd-exposed mice were significantly smaller than controls, an effect rescued by Luteolin (Fig. 2B). Body weight measurements confirmed that Cd reduced weight, while Luteolin treatment mitigated this effect (Fig. 2C). Urine protein assays indicated renal damage in Cd-exposed mice, which was ameliorated by Luteolin, whereas Luteolin alone had no effect (Fig. 2D).

Behavioral assessments were performed post-treatment. In the Y-maze test, Cd-exposed mice exhibited reduced exploration and spatial memory, while Luteolin restored these abilities to control levels (Fig. 2E). The pole test revealed impaired motor coordination in Cd-exposed mice, characterized by frequent falls, but Luteolin improved their performance (Fig. 2F). In the forced swimming test, Cd-exposed mice showed prolonged immobility, indicative of depressive-like behavior, which was reversed by Luteolin (Fig. 2G). Similarly, the tail suspension test showed reduced limb grasps in Cd-exposed mice, a sign of depression, which Luteolin alleviated (Fig. 2H). The open field test further demonstrated that Cd reduced total walking distance and increased freezing time in the central zone, indicating locomotor inhibition and depressive-like behavior. Luteolin restored these behaviors (Fig. 2I and J).

In the Morris water maze (MWM) acquisition phase, Cd-exposed mice exhibited longer escape latencies and more complex paths, but Luteolin improved their performance (Fig. 2K and L). In the probe trial, Cd-exposed mice spent less time in the target quadrant, crossed the platform location fewer times, and swam shorter distances, with no change in swimming speed. Luteolin restored these deficits, indicating improved learning and memory (Fig. 2M and N). In summary, Luteolin alleviated Cd-induced motor, cognitive, and depressive-like behaviors in mice.

3.3. Luteolin attenuated systemic tissue damage induced by cd in mice

Luteolin's restoration of behavioral deficits prompted us to investigate its effects on tissue damage. Organ weights revealed that Cd increased the liver and brain organ indices but decreased the kidney

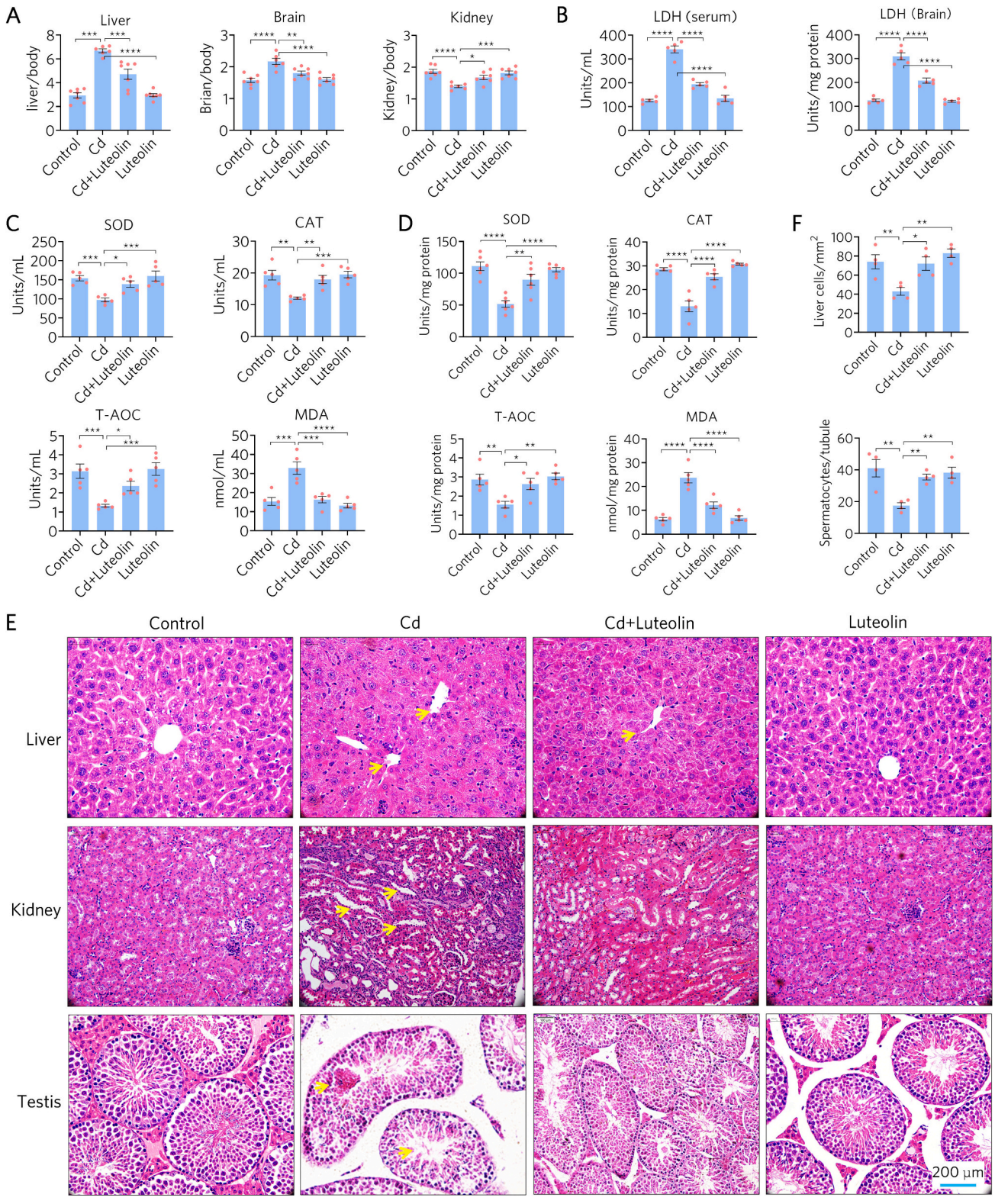

Fig. 3. Luteolin attenuated systemic tissue injury induced by Cd in mice.
(A) Organ indices (organ-to-body weight ratios) for liver, brain, and kidney. Cd exposure caused hepatic edema, cerebral edema, and renal atrophy, as indicated by changes in organ indices. However, Luteolin ameliorated these changes. (B) LDH activity in serum and brain, measured using an LDH assay kit. Luteolin reversed the Cd-induced increase in LDH activity. (C) Serum levels of antioxidant enzymes (SOD, CAT), total antioxidant capacity (T-AOC), and lipid peroxidation product (MDA), measured using commercial kits. (D) SOD and CAT enzymatic activities, T-AOC and MDA levels in brain tissue were measured with kits. (E) H & E staining of liver, kidney and testicular tissues. Luteolin ameliorated Cd-induced tissue damage. (F) Quantification of liver cells and spermatocytes in (E). Arrows indicate pathological changes in Cd-exposed tissues. Statistical analysis was performed using one-way ANOVA followed by Dunnett's multiple comparison test. n.s, not significant; *, $p < 0.05$; **, $p < 0.01$; ***, $p < 0.001$; ****, $p < 0.0001$.

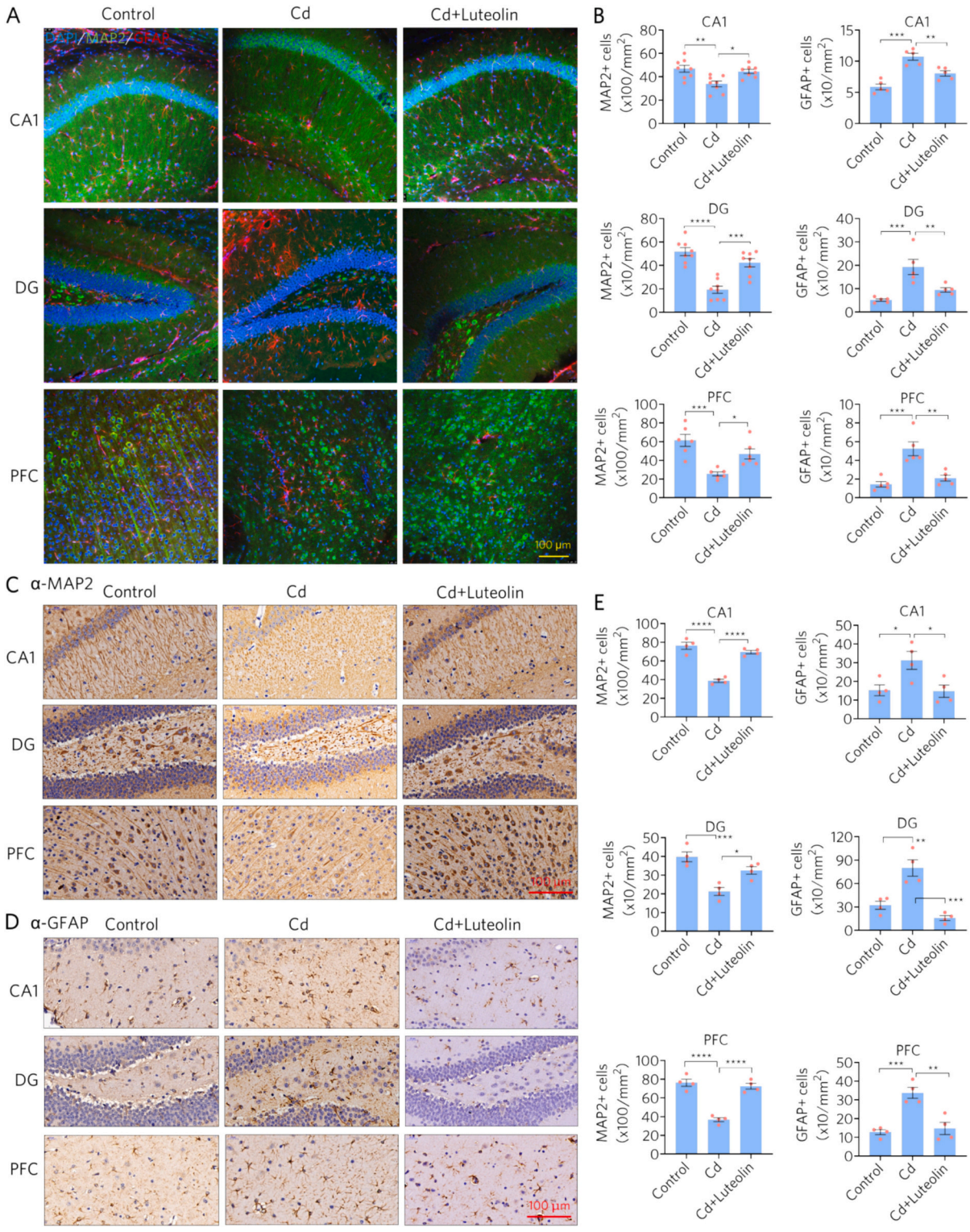

Fig. 4. Luteolin protected neurons and astrocytes from Cd-induced toxicity in mice.
(A) Representative immunofluorescence images of neurons and astrocytes in the hippocampal CA and DG regions and in the PFC, using antibodies specific for MAP2 (for neurons) and GFAP (for astrocytes). Cd-induced brain toxicity was manifested by a reduction in MAP2-positive cells and an increase in GFAP-positive cells, accompanied by morphological alterations. Luteolin significantly attenuated Cd-induced neurotoxicity. (B) Quantitative analysis of the number of MAP2- or GFAP-positive cells in the hippocampus and PFC, based on the images in (A). (C) Representative IHC images of neurons in the hippocampal CA and DG regions and PFC using an antibody specific for MAP2. Cd-induced toxicity in the brain was manifested by a decrease in MAP2-positive cells and their morphological changes. However, Luteolin attenuated Cd-induced neurotoxicity. (D) Representative IHC images of astrocytes in the hippocampal CA and DG regions and PFC using a GFAP-specific antibody. Cd-induced brain toxicity was marked by an increase in GFAP-positive cells, which was alleviated by Luteolin. (E) Quantification of MAP2- or GFAP-positive cells based on the images in (C) and (D). In this figure, data are expressed as mean ± s.e.m. and one-way ANOVA followed by Dunnett's multiple comparison tests was performed. n.s, not significant; *, $p < 0.05$; **, $p < 0.01$; ***, $p < 0.001$; ****, $p < 0.0001$.

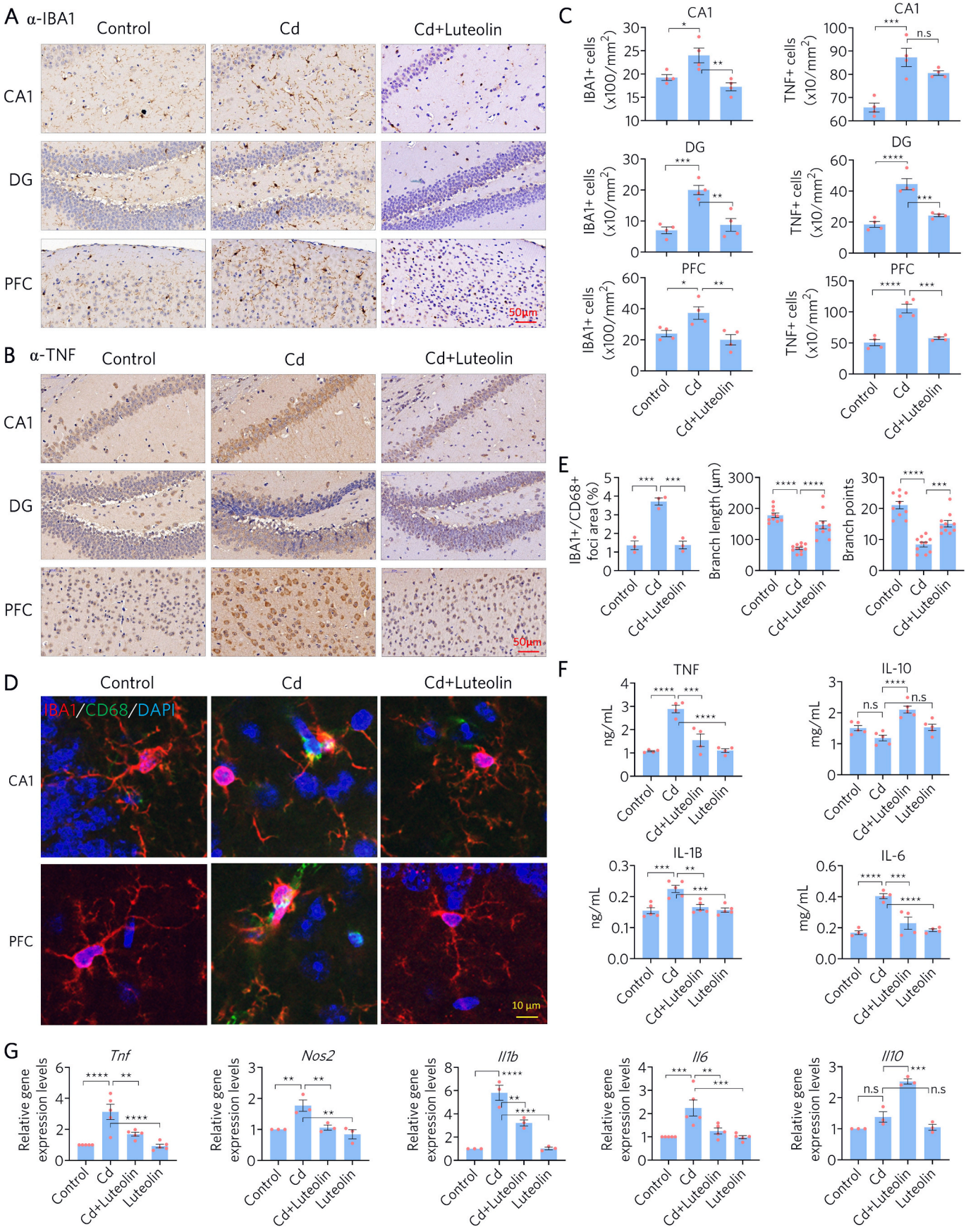

(caption on next page)

Fig. 5. Luteolin ameliorates Cd-induced microglia activation and inflammation in the mouse brain. (A-B) Representative IHC images of microglia in the hippocampal CA1 and DG regions as well as in the PFC, using an antibody specific for IBA1 or TNF. Cd-induced toxicity in the brain was manifested by an increase in IBA1- or TNF- positive cells. However, Luteolin attenuated the Cd-induced microglia activation. (C) Quantification of IBA1- or TNF-positive cells based on the images in (A) and (B). (D) Representative immunofluorescence (IF) images of microglia using antibodies specific for IBA1 and CD68. Cd toxicity activated microglia, as evidenced by increased levels of CD68 and IBA1. In contrast, Luteolin attenuated Cd-induced upregulation of CD68 and microglial activation. (E) Microglial activation was assessed by counting IBA1- or CD68-positive cells and measuring branch lengths and branch points of IBA1-positive cells. (F) Serum levels of pro-inflammatory factors (TNF, IL-1B, IL-6) and the anti-inflammatory factor IL-10 were measured by ELISA. (G) mRNA levels of pro-inflammatory factors (*Tnf*, *Il1b*, *Il6*, *Il10* and *Nos2*) in brain tissue were detected by RT-PCR. In this figure, data are expressed as mean ± s.e.m. and one-way ANOVA followed by Dunnett's multiple comparison tests was performed. n.s, not significant; *, $p < 0.05$; **, $p < 0.01$; ***, $p < 0.001$; ****, $p < 0.0001$.

index, effects reversed by Luteolin, suggesting it inhibits Cd-induced liver/brain hyperplasia and kidney atrophy (Fig. 3A). Cd elevated serum and brain LDH activity, indicating tissue damage, which Luteolin reduced (Fig. 3B). Cd also decreased total antioxidant capacity (T-AOC) and antioxidant enzymes (SOD, CAT) while increasing lipid peroxidation (MDA) in serum and brain. Luteolin restored oxidative stress levels (Fig. 3C and D). H&E staining confirmed Cd-induced tissue damage (Fig. 3E), as seen in liver congestion, hepatocyte loss, and inflammatory infiltration; renal tubular swelling and luminal narrowing; and testicular spermatogonial detachment and reduced spermatocytes. Luteolin ameliorated these pathologies (Fig. 3E and F). These findings suggest Luteolin mitigates Cd-induced oxidative stress and tissue damage.

3.4. Luteolin protects neurons and astrocytes from cd-induced toxicity in vivo

To explore the cellular mechanisms underlying histological changes, we performed immunofluorescence (IF) and immunohistochemistry (IHC) staining on the brain sections (Fig. 4). IF results identifying neurons with MAP2 antibody showed that the number of MAP2-positive neurons was reduced in the CA1 ($p = 0.0023$) and DG ($p < 0.0001$) regions of the hippocampus and PFC ($p = 0.0003$) of Cd-treated mice, but was recovered in mice co-administered with Luteolin (Fig. 4A and B). Conversely, GFAP staining revealed increased astrocytes in these regions, attenuated by Luteolin (Fig. 4A and B). IHC confirmed these findings, showing decreased MAP2-positive neurons and increased GFAP-positive astrocytes in Cd-exposed mice, both reversed by Luteolin (Fig. 4C-4E). Thus, Luteolin maintains normal histology by countering Cd-induced cellular changes.

3.5. Luteolin ameliorated cd-induced glial activation and inflammation in mouse brain

IHC staining for IBA1 showed that Cd-intoxication enhanced the cell number of IBA1-positive microglia in the CA1 and DG regions of the hippocampus, and in the PFC region, which Luteolin attenuated this change (Fig. 5A). Correspondingly, TNF-positive cells increased with Cd exposure but were reduced by Luteolin ($p = 0.002$) (Fig. 5B-C). For Cd-induced microglia proliferation and activation, we performed IF staining of CD68, IF staining for CD68, a marker of microglial phagocytic activity, in brain sections of hippocampus and PFC, and revealed increased IBA1/CD68 double-positive cells with enlarged cell bodies and short protrusions in Cd-exposed mice. Luteolin restored microglial morphology and reduced activation (Fig. 5D and E). Consistently, the inflammatory factors TNF, IL-1B, and IL-6 assayed by ELISA were increased in serum and brain, while IL-10 (an anti-inflammatory cytokine) was reduced (Fig. 5F). Moreover, gene expression of these inflammatory factors as well as *Nos2* by RT-PCR confirmed these changes in brain upon Cd-induced toxicity (Fig. 5G). However, Luteolin restored these inflammatory and oxidative stress markers (Fig. 5F and G). Thus, Luteolin mitigates Cd-induced neuroinflammation by inhibiting microglial activation.

3.6. Luteolin restores the Notch1/Hes1 and BDNF-TrkB/AKT1 signaling axes to mitigate cd toxicity in mice

To elucidate the molecular mechanisms, we examined protein expression by Western blot. Firstly, we monitored the protein expression of MAP2, GFAP, and IBA1 in the hippocampus. Cd reduced MAP2 and increased GFAP and IBA1 in the hippocampus, indicating neuronal loss and glial activation, which Luteolin reversed (Fig. 6A). We then examined the protein level of BDNF-TrkB/AKT1 pathways, which regulates

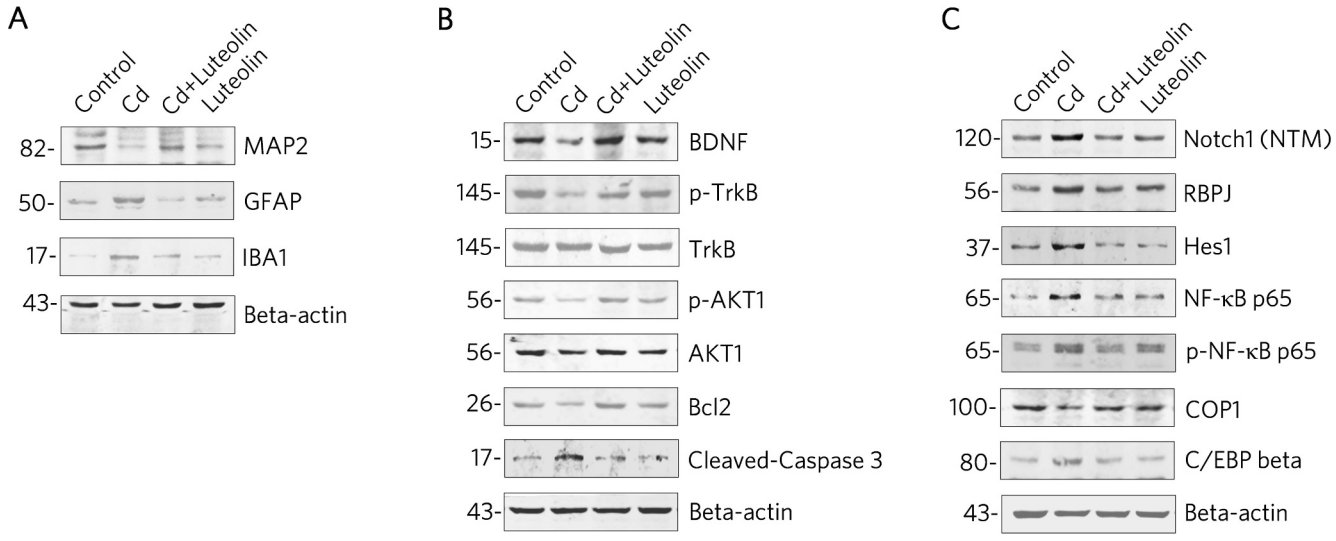

Fig. 6. Luteolin restores the Notch1/Hes1 and BDNF-TrkB/AKT1 signaling axes to mitigate Cd-induced toxicity in the hippocampus. (A) Western blot analysis of MAP2, GFAP, and IBA1 protein levels. (B) Western blot detection of proteins involved in the BDNF-TrkB/AKT1 signaling axis and apoptotic markers Bcl2 and cleaved-Caspase 3. (C) Western blot analysis of proteins in the Notch1/Hes1 signaling axis.

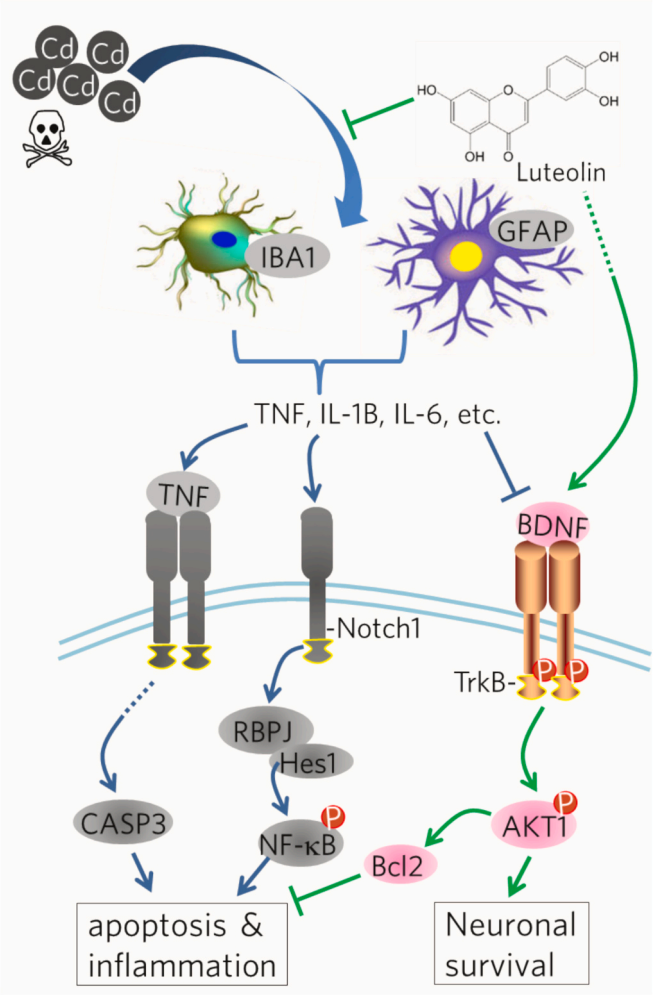

Fig. 7. Schematic illustration of Luteolin's attenuation of Cd-induced toxicity by restoring of the Notch1/Hes1 and BDNF-TrkB/AKT1 signaling axes. Cd induces inflammatory activation in glial cells (e.g., microglia and astrocytes), leading to the release of pro-inflammatory factors, such as TNF, IL-1B, and IL-6. These factors in turn activate cellular inflammatory and apoptotic signaling pathways, including Notch1/RBPJ/NF-κB, triggering neuroinflammation and neuronal death. Conversely, Luteolin inhibits Cd-induced toxicity by promoting BDNF-mediated TrkB/AKT1 signaling pathway, thereby inhibiting inflammation and enhancing neuronal survival.

neuronal survival and inhibits apoptosis. Cd downregulated BDNF, p-TrkB, p-AKT1, and Bcl2 while upregulating cleaved-Caspase 3, effects restored by Luteolin (Fig. 6B). Corresponding, the Notch1/Hes1 signaling axis, which mediates neuronal inflammation, was activated by Cd toxicity, as protein levels of Notch1, Hes1, RBPJ, as well as NF-κB and its phosphorylated form on Ser536 were increased (Fig. 6C), indicating that inflammatory responses mediated by NF-κB pathway, were activated after Cd toxicity. In addition, COP1, the E3 ubiquitin ligase of C/EBP beta in protein degradation, was also reduced, which corresponds to the upregulation of C/EBP beta, a transcriptional regulator of inflammatory factors. However, Luteolin treatment restored the expression of COP1 and C/EBP beta, thereby suppressing inflammation (Fig. 6C). In conclusion, Luteolin inhibits neuroinflammation by suppressing the Notch1/Hes1 signaling axis and promotes neuronal survival by restoring the BDNF-TrkB/AKT1 pathway, thereby mitigating Cd-induced systemic toxicity (Fig. 7).

4. Discussion

In this study, we systematically investigated the effects of Cd toxicity on cultured cells and mouse models, as well as the neuroprotective of Luteolin against Cd-induced toxicity. In hippocampal neurons and glial cells, Luteolin demonstrated protective effects against Cd-induced toxicity by restoring the BDNF-TrkB/AKT1 signaling axis, thereby inhibiting apoptosis and neuroinflammation (Fig. 1). In mouse models, Cd toxicity not only caused damage to the brain, liver, kidneys, and testes (Fig. 2 and Fig. 3) but also significantly impaired motor activity, learning and memory abilities, and induced depression-like behaviors. These findings underscore Cd as a critical environmental risk factor for neurodegenerative diseases such as Alzheimer's disease (AD). The AD-like symptoms induced by Cd, including learning and memory impairments, are comparable to those induced by $AlCl_3$/Gal [42,43]. Luteolin, a natural flavonoid, has recently emerged as a promising candidate in the field of neuroprotection [20,44]. The novelty of this study lies in its comprehensive exploration of luteolin's protective effects against Cd-induced neurotoxicity and the elucidation of its molecular mechanisms through the restoration of the BDNF-TrkB/AKT1 and Notch1/Hes1 signaling axes (Figs. 1 and 6).

The central nervous system (CNS) comprises two main cell types: neurons and glial cells. Neurons, the fundamental units of the brain and nervous system, are primarily responsible for neurodegenerative diseases when dysfunctional or lost [45,46]. Glial cells, including microglia and astrocytes, play a pivotal role in the inflammatory response within the neuronal system [47,48]. As non-neural cells, glial cells can promote the proliferation and survival of CNS cells by releasing specific growth factors, as well as facilitate the death of unwanted cells by secreting cytotoxins [47]. Conversely, adverse activation of glial cells can exacerbate inflammation and influence the onset and progression of neurodegenerative diseases, including AD [49]. In this study, we observed that Cd toxicity induced the proliferation and activation of astrocytes and microglia, accompanied by neuronal death. Microglia, the primary immune cells in the CNS, are responsible for recognizing and removing damaged nerves, plaques, and infectious materials, thereby maintaining CNS homeostasis [50]. However, hyperactivation of microglia can trigger inflammatory responses through the excessive release of inflammatory factors and oxidative substances, leading to neuronal damage and neurotoxicity [51,52]. Elevated levels of activated microglia and inflammatory factors such as TNF, IL-1B, and IL-6 have been detected in the brains of APP transgenic mice and AD patients [53]. Thus, Cd toxicity and AD share similar glial and neuronal alterations. Studies have shown that Cd toxicity activates the Notch1/Hes1 signaling axis and triggers an inflammatory response, while inhibiting the BDNF-TrkB/AKT1 signaling axis and impairing neuronal survival. However, our findings suggest that Luteolin can attenuate Cd-induced neuronal toxicity and improve mouse behavior through these molecular mechanisms, indicating its potential therapeutic role in neuronal disorders, including AD and depression.

Indeed, Luteolin has demonstrated significant neuroprotective effects in various models of neuronal injury and neurodegenerative diseases. In traumatic brain injury models, Luteolin ameliorates secondary brain injury by reducing oxidative stress, neuronal apoptosis, and inflammation through the activation of the Nrf2-ARE pathway [54]. In the context of preventing amyloid-beta deposits and tau tangles, luteolin may improve brain insulin sensitivity and reduce neuroinflammation [26]. Additionally, Luteolin protects dopaminergic neurons by inhibiting microglial activation and reducing the production of pro-inflammatory cytokines [44]. Notably, Luteolin may directly bind to PPARγ (peroxisome proliferator-activated receptor), enhancing its function, as the deletion of PPARγ activity abolishes luteolin's effects on AD pathology [26]. Furthermore, Luteolin can interact with NGF (neuronal growth factor), stimulating NGF-induced neurite outgrowth and potentiating its receptor signaling [55]. Our study further confirms that Luteolin enhances the activity of the BDNF-TrkB/AKT1 signaling

pathway, potentially through direct interaction with NGF, which activates the TrkB/AKT1 signaling axis, resulting in a positive feedback loop that promotes BDNF gene expression (Fig. 1E and Fig. 6B).

Despite the promising neuroprotective effects of Luteolin, research in this area is still in its early stages, and several limitations remain. First, the metabolic pathways and the form in which Luteolin enters the CNS are not fully understood. Due to the presence of multiple phenolic hydroxyl groups in its molecular structure, Luteolin is highly hydrophilic, which may limit its ability to directly cross the BBB. Second, the bioavailability of Luteolin is relatively low, and improving its bioavailability and optimizing its delivery methods are important directions for future research. Furthermore, the long-term safety and personalized therapeutic potential of Luteolin require further exploration. Finally, whether Luteolin's neuroprotective effects are primarily due to its antioxidant activity or its direct interaction with cellular targets to specifically modulate signaling pathways remains to be thoroughly investigated.

In conclusion, Luteolin, as a potential neuromodulator, holds significant promise in neuroprotection and drug development. However, studies are needed to clarify its molecular mechanisms, metabolic pathways, and bioavailability, as well as evaluate its long-term safety and clinical application potential.

CRediT authorship contribution statement

Hui-Yong Ma: Software, Methodology, Investigation, Data curation. **Jing Wang:** Software, Methodology, Investigation. **Jun Wang:** Validation, Methodology, Investigation. **Zhe Guo:** Methodology, Investigation, Funding acquisition. **Xiao-Yan Qin:** Validation, Project administration, Funding acquisition. **Rongfeng Lan:** Writing – review & editing, Writing – original draft, Data curation. **Yang Hu:** Validation, Project administration, Methodology.

Declaration of competing interest

The authors declare that they have no known competing financial interests or personal relationships that could have appeared to influence the work reported in this paper.

Data availability

Data will be made available on request.

Acknowledgments

This study was supported by the Academic Team Leadership Program of Minzu University of China (2023QNYL16, 2024XSYL02) and the Scientific Research Program of Guangxi Administration of Traditional Chinese Medicine (GXZYA20240474).

References

[1] ATSDR, Agency for Toxic Substances and Disease Registry, ATSDR's 2022 Substance Priority List, 2022.
[2] J.J.V. Branca, M. Maresca, G. Morucci, T. Mello, M. Becatti, L. Pazzagli, I. Colzi, C. Gonnelli, D. Carrino, F. Paternostro, C. Nicoletti, C. Ghelardini, M. Gulisano, L. Di Cesare Mannelli, A. Pacini, Effects of cadmium on ZO-1 tight junction integrity of the blood brain barrier, Int. J. Mol. Sci. 20 (23) (2019).
[3] T. Zhang, Z. Xu, L. Wen, D. Lei, S. Li, J. Wang, J. Huang, N. Wang, C. Durkan, X. Liao, G. Wang, Cadmium-induced dysfunction of the blood-brain barrier depends on ROS-mediated inhibition of PTPase activity in zebrafish, J. Hazard. Mater. 412 (2021) 125198.
[4] K.M. Bakulski, Y.A. Seo, R.C. Hickman, D. Brandt, H.S. Vadari, H. Hu, S.K. Park, Heavy metals exposure and Alzheimer's disease and related dementias, J. Alzheimers Dis. 76 (4) (2020) 1215–1242.
[5] K.N. Kim, M.R. Lee, Y.H. Choi, B.E. Lee, Y.C. Hong, Associations of blood cadmium levels with depression and lower handgrip strength in a community-dwelling elderly population: a repeated-measures panel study, J. Gerontol. A Biol. Sci. Med. Sci. 71 (11) (2016) 1525–1530.
[6] K. Raj, P. Kaur, G.D. Gupta, S. Singh, Metals associated neurodegeneration in Parkinson's disease: Insight to physiological, pathological mechanisms and management, Neurosci. Lett. 753 (2021) 135873.
[7] K. Gustin, F. Tofail, M. Vahter, M. Kippler, Cadmium exposure and cognitive abilities and behavior at 10 years of age: A prospective cohort study, Environ. Int. 113 (2018) 259–268.
[8] Z. Li, Y. Liu, X. Li, W. Ju, G. Wu, X. Yang, X. Fu, X. Gao, Association of Elements with schizophrenia and intervention of selenium supplements, Biol. Trace Elem. Res. 183 (1) (2018) 16–21.
[9] K. Rezaei, G. Mastali, E. Abbasgholinejad, M.A. Bafrani, A. Shahmohammadi, Z. Sadri, M.A. Zahed, Cadmium neurotoxicity: Insights into behavioral effect and neurodegenerative diseases, Chemosphere 364 (2024) 143180.
[10] T.J. Huat, J. Camats-Perna, E.A. Newcombe, N. Valmas, M. Kitazawa, R. Medeiros, Metal toxicity links to Alzheimer's disease and Neuroinflammation, J. Mol. Biol. 431 (9) (2019) 1843–1868.
[11] L. Che, C.L. Yang, Y. Chen, Z.L. Wu, Z.B. Du, J.S. Wu, C.L. Gan, S.P. Yan, J. Huang, N.J. Guo, Y.C. Lin, Z.N. Lin, Mitochondrial redox-driven mitofusin 2 S-glutathionylation promotes neuronal necroptosis via disrupting ER-mitochondria crosstalk in cadmium-induced neurotoxicity, Chemosphere 262 (2021) 127878.
[12] Y. Ma, Q. Su, C. Yue, H. Zou, J. Zhu, H. Zhao, R. Song, Z. Liu, The effect of oxidative stress-induced autophagy by cadmium exposure in kidney, liver, and bone damage, and neurotoxicity, Int. J. Mol. Sci. 23 (21) (2022).
[13] D. Cui, Y. Chen, B. Ye, W. Guo, D. Wang, J. He, Natural products for the treatment of neurodegenerative diseases, Phytomedicine 121 (2023) 155101.
[14] S.S. Bharate, S. Mignani, R.A. Vishwakarma, Why are the majority of active compounds in the CNS domain natural products? A Critical Analysis, J. Med. Chem. 61 (23) (2018) 10345–10374.
[15] J.Y. Yang, J. Wang, Y. Hu, D.Y. Shen, G.L. Xiao, X.Y. Qin, R.F. Lan, Paeoniflorin improves cognitive dysfunction, restores glutamate receptors, attenuates gliosis and maintains synaptic plasticity in cadmium-intoxicated mice, Arab. J. Chem. 16 (1) (2023).
[16] X.M. Shu, Y. Hu, X. Fang, J. Wang, X.Y. Qin, R. Lan, Salidroside alleviates cadmium-induced toxicity in mice by restoring the notch/HES-1 and RIP1-driven inflammatory signaling axis, Inflamm. Res. 71 (5–6) (2022) 615–626.
[17] T. Boeing, P. de Souza, S. Speca, L.B. Somensi, L.N.B. Mariano, B.J. Cury, M. Ferreira Dos Anjos, N.L.M. Quintao, L. Dubuqoy, P. Desreumax, L.M. da Silva, S. F. de Andrade, Luteolin prevents irinotecan-induced intestinal mucositis in mice through antioxidant and anti-inflammatory properties, Br. J. Pharmacol. 177 (10) (2020) 2393–2408.
[18] J.W. Daily, S. Kang, S. Park, Protection against Alzheimer's disease by luteolin: Role of brain glucose regulation, anti-inflammatory activity, and the gut microbiota-liver-brain axis, Biofactors 47 (2) (2021) 218–231.
[19] W. Fan, S. Qian, P. Qian, X. Li, Antiviral activity of luteolin against Japanese encephalitis virus, Virus Res. 220 (2016) 112–116.
[20] S.F. Nabavi, N. Braidy, O. Gortzi, E. Sobarzo-Sanchez, M. Daglia, K. Skalicka-Wozniak, S.M. Nabavi, Luteolin as an anti-inflammatory and neuroprotective agent: A brief review, Brain Res. Bull. 119 (Pt A) (2015) 1–11.
[21] T. Zhang, W. Wu, D. Li, T. Xu, H. Zhu, D. Pan, S. Zhu, Y. Liu, Anti-oxidant and anti-apoptotic effects of luteolin on mice peritoneal macrophages stimulated by angiotensin II, Int. Immunopharmacol. 20 (2) (2014) 346–351.
[22] Y. Wang, H. Su, X. Song, S.S. Fiati Kenston, J. Zhao, Y. Gu, Luteolin inhibits multi-heavy metal mixture-induced HL7702 cell apoptosis through downregulation of ROS-activated mitochondrial pathway, Int. J. Mol. Med. 41 (1) (2018) 233–241.
[23] L. Qin, Z. Chen, L. Yang, H. Shi, H. Wu, B. Zhang, W. Zhang, Q. Xu, F. Huang, X. Wu, Luteolin-7-O-glucoside protects dopaminergic neurons by activating estrogen-receptor-mediated signaling pathway in MPTP-induced mice, Toxicology 426 (2019) 152256.
[24] Z. Elmazoglu, A.S. Yar Saglam, C. Sonmez, C. Karasu, Luteolin protects microglia against rotenone-induced toxicity in a hormetic manner through targeting oxidative stress response, genes associated with Parkinson's disease and inflammatory pathways, Drug Chem. Toxicol. 43 (1) (2020) 96–103.
[25] R. Couture, N. Mora, S. Al Bittar, M. Najih, M. Touaibia, L.J. Martin, Luteolin modulates gene expression related to steroidogenesis, apoptosis, and stress response in rat LC540 tumor Leydig cells, Cell Biol. Toxicol. 36 (1) (2020) 31–49.
[26] Z. He, X. Li, Z. Wang, Y. Cao, S. Han, N. Li, J. Cai, S. Cheng, Q. Liu, Protective effects of luteolin against amyloid beta-induced oxidative stress and mitochondrial impairments through peroxisome proliferator-activated receptor gamma-dependent mechanism in Alzheimer's disease, Redox Biol. 66 (2023) 102848.
[27] S.R. Fan, T.T. Ren, M.Y. Yun, R. Lan, X.Y. Qin, Edaravone attenuates cadmium-induced toxicity by inhibiting oxidative stress and inflammation in ICR mice, Neurotoxicology 86 (2021) 1–9.
[28] T.T. Ren, J.Y. Yang, J. Wang, S.R. Fan, R. Lan, X.Y. Qin, Gisenoside Rg1 attenuates cadmium-induced neurotoxicity in vitro and in vivo by attenuating oxidative stress and inflammation, Inflamm. Res. 70 (10–12) (2021) 1151–1164.
[29] R.Y. Pan, J. Ma, H.T. Wu, Q.S. Liu, X.Y. Qin, Y. Cheng, Neuroprotective effects of a Coeloglossum viride var. Bracteatum extract in vitro and in vivo, Sci. Rep. 7 (1) (2017) 9209.
[30] Z.P. Cai, C. Cao, Z. Guo, Y. Yu, S.J. Zhong, R.Y. Pan, H. Liang, R. Lan, X.Y. Qin, Coeloglossum viride var. bracteatum extract attenuates staurosporine induced neurotoxicity by restoring the FGF2-PI3K/Akt signaling axis and Dnmt3, Heliyon 7 (7) (2021) e07503.
[31] J. Wang, Q.T. Liu, D.Y. Shen, J.P. Bai, Y. Hu, Q. Huang, H.J. Yu, N.N. He, X.Y. Qin, R. Lan, Network pharmacology analysis of the active ingredients of Corydalis hendersonii Hemsl. And their effects on eliminating neuroinflammation and improving motor functions in MPTP-intoxicated mice, J. Ethnopharmacol. 318 (Pt B) (2024) 117009.

[32] L. Xue, X. Jin, T. Ji, R. Li, X. Zhuge, F. Xu, Z. Quan, H. Tong, W. Yu, Luteolin ameliorates DSS-induced colitis in mice via suppressing macrophage activation and chemotaxis, Int. Immunopharmacol. 124 (Pt B) (2023) 110996.
[33] J.J. Kou, J.Z. Shi, Y.Y. He, J.J. Hao, H.Y. Zhang, D.M. Luo, J.K. Song, Y. Yan, X. M. Xie, G.H. Du, X.B. Pang, Luteolin alleviates cognitive impairment in Alzheimer's disease mouse model via inhibiting endoplasmic reticulum stress-dependent neuroinflammation, Acta Pharmacol. Sin. 43 (4) (2022) 840–849.
[34] X.X. Li, X.Y. Lang, T.T. Ren, J. Wang, R. Lan, X.Y. Qin, Coeloglossum viride var. bracteatum extract attenuates Aβ-induced toxicity by inhibiting RIP1-driven inflammation and necroptosis, J. Ethnopharmacol. 282 (2022) 114606.
[35] S.J. Zhong, L. Wang, H.T. Wu, R. Lan, X.Y. Qin, Coeloglossum viride var. bracteatum extract improves learning and memory of chemically-induced aging mice through upregulating neurotrophins BDNF and FGF2 and sequestering neuroinflammation, J. Funct. Foods 57 (2019) 40–47.
[36] T.T. Ren, J.Y. Yang, J. Wang, S.R. Fan, R. Lan, X.Y. Qin, Gisenoside Rg1 attenuates cadmium-induced neurotoxicity in vitro and in vivo by attenuating oxidative stress and inflammation, Inflamm. Res. 70 (10–12) (2021) 1151–1164.
[37] H.C. Yan, X. Cao, M. Das, X.H. Zhu, T.M. Gao, Behavioral animal models of depression, Neurosci. Bull. 26 (4) (2010) 327–337.
[38] X.G. Gong, H.M. Sun, Y. Zhang, S.J. Zhang, Y.S. Gao, J. Feng, J.H. Hu, C. Gai, Z. Y. Guo, H. Xu, L. Ma, Da-bu-yin-wan and qian-zheng-san to neuroprotect the mouse model of Parkinson's disease, Evid. Based Complement. Alternat. Med. 2014 (2014) 729195.
[39] J. Ruan, Y. Yao, Behavioral tests in rodent models of stroke, Brain Hemorrhages 1 (4) (2020) 171–184.
[40] D.A. Christakis, J.S. Ramirez, J.M. Ramirez, Overstimulation of newborn mice leads to behavioral differences and deficits in cognitive performance, Sci. Rep. 2 (2012) 546.
[41] Z. Guo, J.P. Bai, J. Wang, X.Y. Lang, M.M. Cao, S.J. Zhong, L. Cui, Y. Hu, X.Y. Qin, R.F. Lan, Coeloglossum viride var. bracteatum attenuates lipopolysaccharide-induced acute depressive-like behaviors in mice by inhibiting neuroinflammation and protecting synaptic plasticity, J. Funct. Foods 122 (2024).
[42] F. Xiao, L.I. Xiao-Guang, X.Y. Zhang, J.D. Hou, L.F. Lin, Q. Gao, H.M. Luo, D.O. Pharmacology, S.O. Medicine, J. University, Combined administration of D-galactose and aluminium induces Alzheimer-like lesions in brain, Neurosci. Bull. 27 (3) (2011) 143–155.
[43] Y. Hu, X. Fang, J. Wang, T.T. Ren, Y.Y. Zhao, J.F. Dai, X.Y. Qin, R. Lan, Astragalin attenuates AlCl3/D-galactose-induced aging-like disorders by inhibiting oxidative stress and neuroinflammation, Neurotoxicology 91 (2022) 60–68.
[44] H.Q. Chen, Z.Y. Jin, X.J. Wang, X.M. Xu, L. Deng, J.W. Zhao, Luteolin protects dopaminergic neurons from inflammation-induced injury through inhibition of microglial activation, Neurosci. Lett. 448 (2) (2008) 175–179.
[45] H. Chi, H.Y. Chang, T.K. Sang, Neuronal cell death mechanisms in major neurodegenerative diseases, Int. J. Mol. Sci. 19 (10) (2018).
[46] M.T. Heemels, Neurodegenerative diseases, Nature 539 (7628) (2016) 179.
[47] N.J. Allen, D.A. Lyons, Glia as architects of central nervous system formation and function, Science 362 (6411) (2018) 181–185.
[48] Y.S. Kim, J. Choi, B.E. Yoon, Neuron-glia interactions in neurodevelopmental disorders, Cells 9 (10) (2020).
[49] H.S. Kwon, S.H. Koh, Neuroinflammation in neurodegenerative disorders: the roles of microglia and astrocytes, Transl Neurodegener 9 (1) (2020) 42.
[50] A. Reiner, J. Levitz, Glutamatergic signaling in the central nervous system: ionotropic and metabotropic receptors in concert, Neuron 98 (6) (2018) 1080–1098.
[51] D.V. Hansen, J.E. Hanson, M. Sheng, Microglia in Alzheimer's disease, J. Cell Biol. 217 (2) (2018) 459–472.
[52] M. Prinz, S. Jung, J. Priller, Microglia biology: one century of evolving concepts, Cell 179 (2) (2019) 292–311.
[53] J.C. Magee, C. Grienberger, Synaptic plasticity forms and functions, Annu. Rev. Neurosci. 43 (2020) 95–117.
[54] J. Xu, H. Wang, K. Ding, L. Zhang, C. Wang, T. Li, W. Wei, X. Lu, Luteolin provides neuroprotection in models of traumatic brain injury via the Nrf2-ARE pathway, Free Radic. Biol. Med. 71 (2014) 186–195.
[55] A. Xiong Gao, T.C. Xia, M. Shing-Hung Mak, K. Kin-Leung Kwan, B. Zhong-Yu Zheng, J. Xiao, T.T. Dong, K.W. Tsim, Luteolin stimulates the NGF-induced neurite outgrowth in cultured PC12 cells through binding with NGF and potentiating its receptor signaling, Food Funct. 12 (22) (2021) 11515–11525.